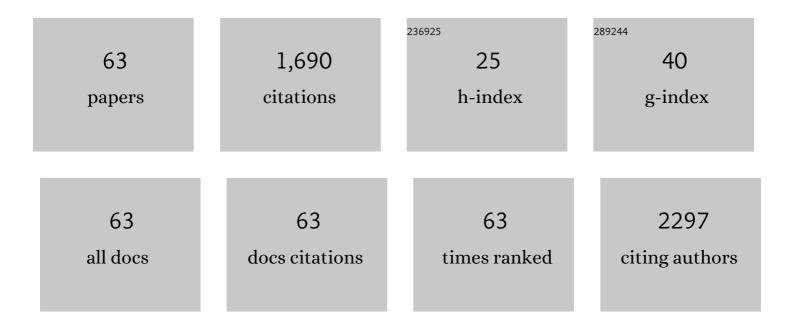
Heqing Yang

List of Publications by Year in descending order

Source: https://exaly.com/author-pdf/5523475/publications.pdf Version: 2024-02-01



HEOING YANG

#	Article	IF	CITATIONS
1	Enhanced sensitivity of hydrogenated α-Fe2O3 nanoplates having {001} facets and the gas sensing mechanism. Journal of Materials Science: Materials in Electronics, 2022, 33, 3617-3630.	2.2	1
2	Enhanced visible-light photocatalytic activity of hydrogenated Fe3O4 nanooctahedrons with {111} polar facets in degradation of Basic Fuchsin and the photocatalytic mechanism. Journal of Materials Science: Materials in Electronics, 2022, 33, 13095-13109.	2.2	1
3	Photogenerated Charge Separation between Polar Crystal Facets Under a Spontaneous Electric Field. Advanced Optical Materials, 2021, 9, 2001898.	7.3	7
4	Enhanced gas sensing performances of hydrogenated MnO octahedrons with {111} facets and the sensing mechanism of unsaturated Mn as a reactive atom. Journal of Alloys and Compounds, 2021, 884, 160872.	5.5	4
5	Effect of 8-coordinated Pb atom density at (001) surface on sensitivity in PbTiO3 nanosheets with polar {001} facets and gas sensing mechanism. Journal of Alloys and Compounds, 2021, 887, 161325.	5.5	1
6	Enhanced Sensitivity of Hydrogenated Cu _{0.27} Co _{2.73} O ₄ Nanooctahedrons Having {111} Facets and the Sensing Mechanism of 3-Coordinated Co/Cu Atoms as Active Centers. Langmuir, 2021, 37, 12802-12811.	3.5	2
7	Enhancing gas sensitivity of CdO octahedrons having {111} facets by hydrogenation and sensing mechanism of 3-coordinated Cd atoms as the reactive centers. Applied Surface Science, 2020, 506, 144868.	6.1	9
8	Increasing gas sensitivity of Co3O4 octahedra by tuning Co-Co3O4 (111) surface structure and sensing mechanism of 3-coordinated Co atom as an active center. Journal of Materials Science: Materials in Electronics, 2020, 31, 8852-8864.	2.2	6
9	Hydrogenated Cu2O octahededrons with exposed {111} facets: Enhancing sensing performance and sensing mechanism of 1-coordinated Cu atom as a reactive center. Sensors and Actuators B: Chemical, 2020, 310, 127827.	7.8	22
10	Enhancing gas-sensing property and sensing mechanism at molecule level of the hollow microspheres assembled with ZnO nanoflakes exposing {001} facets. Journal of Materials Science: Materials in Electronics, 2020, 31, 6118-6129.	2.2	7
11	Enhanced response of hydrogenated Fe2O3 nanostructured materials to volatile organic compound vapors and gas sensing mechanism. Journal of Alloys and Compounds, 2019, 806, 705-716.	5.5	8
12	Increasing sensitivity of ZnO nanoparticles by hydrogenation and sensing reaction mechanism. Journal of Materials Science: Materials in Electronics, 2019, 30, 17674-17681.	2.2	1
13	Hydrogenated nanotubes/nanowires assembled from TiO ₂ nanoflakes with exposed {111} facets: excellent photo-catalytic CO ₂ reduction activity and charge separation mechanism between (111) and (1Ì,,1Ì,,1Ì,,) polar surfaces. Journal of Materials Chemistry A, 2019, 7, 14761-14775.	10.3	31
14	Effect of TC(002) on the Output Current of a ZnO Thin-Film Nanogenerator and a New Piezoelectricity Mechanism at the Atomic Level. ACS Applied Materials & Interfaces, 2019, 11, 12656-12665.	8.0	27
15	Improving sensing performance of the ZnO foam structure with exposed {001} facets by hydrogenation and sensing mechanism at molecule level. Applied Surface Science, 2019, 479, 646-654.	6.1	22
16	Increasing sensing sensitivity of the Fe-α-Fe2O3 (104) surface by hydrogenation and the sensing reaction molecule mechanism. Sensors and Actuators B: Chemical, 2019, 281, 366-374.	7.8	17
17	Enhanced gas–sensing properties and sensing mechanism of the foam structures assembled from NiO nanoflakes with exposed {1 1 1} facets. Applied Surface Science, 2019, 470, 596-606.	6.1	31
18	Bifunctional Hydroxylamine Hydrochloride Incorporated Perovskite Films for Efficient and Stable Planar Perovskite Solar Cells. ACS Applied Energy Materials, 2018, 1, 900-909.	5.1	81

HEQING YANG

#	Article	IF	CITATIONS
19	Hydrogenated TiO2 nanosheet based flowerlike architectures: Enhanced sensing performances and sensing mechanism. Journal of Alloys and Compounds, 2018, 749, 543-555.	5.5	14
20	Enhanced Visible-Light Photocatalytic H ₂ Evolution in Cu ₂ O/Cu ₂ Se Multilayer Heterostructure Nanowires Having {111} Facets and Physical Mechanism. Inorganic Chemistry, 2018, 57, 8019-8027.	4.0	23
21	Enhancing gas sensing performances and sensing mechanism at atomic and molecule level of WO3 nanoparticles by hydrogenation. Sensors and Actuators B: Chemical, 2018, 273, 1786-1793.	7.8	48
22	The sensing reaction on the Ni-NiO (111) surface at atomic and molecule level and migration of electron. Sensors and Actuators B: Chemical, 2018, 273, 794-803.	7.8	19
23	Enhancing the Sensing Properties of TiO ₂ Nanosheets with Exposed {001} Facets by a Hydrogenation and Sensing Mechanism. Inorganic Chemistry, 2017, 56, 1504-1510.	4.0	50
24	Spatial charge separation between wurtzite CdS polar (0001) and (000 <mml:math) 0="" etqq0="" overlock<="" rgbt="" td="" tj=""><td>5.5</td><td>10</td></mml:math)>	5.5	10
25	visible-light photocatalytic activity. Journal of Alloys and Compounds, 2017, 700, 138-148. Visible-light photocatalysis in CdTe nanoflakes with exposed {111} facets and charge separation between polar CdTe {111}surfaces. Applied Catalysis B: Environmental, 2017, 208, 94-103.	20.2	15
26	The photovoltaic effect in a [001] orientated ZnO thin film and its physical mechanism. RSC Advances, 2017, 7, 9596-9604.	3.6	10
27	Enhanced Gas Sensitivity and Sensing Mechanism of Network Structures Assembled from α-Fe ₂ O ₃ Nanosheets with Exposed {104} Facets. Langmuir, 2017, 33, 8671-8678.	3.5	34
28	Flowerlike Cu ₂ Te architectures constructed from ultrathin nanoflakes as superior dye adsorbents for wastewater treatment. RSC Advances, 2016, 6, 79612-79619.	3.6	9
29	Superior adsorption performance for triphenylmethane dyes on 3D architectures assembled by ZnO nanosheets as thin as â ⁻¹ ⁄41.5 nm. Journal of Hazardous Materials, 2016, 318, 732-741.	12.4	51
30	Synthesis of ultralong NiSe nanobelts and their excellent adsorption properties towards malachite green in water. RSC Advances, 2016, 6, 104173-104182.	3.6	5
31	Responses of three-dimensional porous ZnO foam structures to the trace level of triethylamine and ethanol. Sensors and Actuators B: Chemical, 2016, 223, 650-657.	7.8	39
32	Superior photocatalytic activities of NiO octahedrons with loaded AgCl particles and charge separation between polar NiO {111} surfaces. Applied Catalysis B: Environmental, 2015, 172-173, 165-173.	20.2	41
33	Visible-light photocatalysis in Cu ₂ Se nanowires with exposed {111} facets and charge separation between (111) and (1Ì,,1Ì,,1Ì) polar surfaces. Physical Chemistry Chemical Physics, 2015, 17, 13280-13289. Superior photocatalytic activity of porous wurtzite ZnO nanosheets with exposed {0 0 1} facets and a	2.8	42
34	charge separation model between polar (0 0 1) and (<mml:math) (<="" 0="" 10="" 152="" 50="" etqq0="" overlock="" rgbt="" td="" tf="" tj=""><td>xmlns:mm 12.7</td><td>l="http://wwv 48</td></mml:math)>	xmlns:mm 12.7	l="http://wwv 48
35	Charge separation between wurtzite ZnO polar {0 0 1} surfaces and their enhanced photocatalytic activity. Applied Catalysis B: Environmental, 2015, 163, 189-197.	20.2	102
36	InOCl nanosheets with exposed {001} facets: Synthesis, electronic structure and surprisingly high photocatalytic activity. Applied Catalysis B: Environmental, 2014, 152-153, 390-396.	20.2	13

HEQING YANG

#	Article	IF	CITATIONS
37	Direct growth of ZnO nanodisk networks with an exposed (0001) facet on Au comb-shaped interdigitating electrodes and the enhanced gas-sensing property of polar {0001} surfaces. Sensors and Actuators B: Chemical, 2014, 195, 71-79.	7.8	59
38	Size-dependent optical properties and enhanced visible light photocatalytic activity of wurtzite CdSe hexagonal nanoflakes with dominant {001} facets. Journal of Alloys and Compounds, 2014, 610, 62-68.	5.5	16
39	Synthesis and formation mechanism of flowerlike architectures assembled from ultrathin NiO nanoflakes and their adsorption to malachite green and acid red in water. Chemical Engineering Journal, 2014, 239, 141-148.	12.7	71
40	Hydrothermal fabrication and enhanced photocatalytic activity of hexagram shaped InOOH nanostructures with exposed {020} facets. Applied Catalysis B: Environmental, 2013, 130-131, 178-186.	20.2	39
41	Solvothermal synthesis and enhanced photocatalytic activity of flowerlike nanoarchitectures assembled from anatase TiO2 nanoflakes. Physica E: Low-Dimensional Systems and Nanostructures, 2012, 44, 2110-2117.	2.7	12
42	Synthesis and enhanced photocatalytic activity of monodisperse flowerlike nanoarchitectures assembled from CdS nanoflakes with exposed {001} facets. Materials Research Bulletin, 2012, 47, 3070-3077.	5.2	27
43	Synthesis and sensing properties of spherical flowerlike architectures assembled with SnO2 submicron rods. Sensors and Actuators B: Chemical, 2012, 173, 643-651.	7.8	105
44	Hydrothermal Synthesis and Magnetic Properties of Fe3O4 Octahedral Microcrystals. Synthesis and Reactivity in Inorganic, Metal Organic, and Nano Metal Chemistry, 2012, 42, 732-735.	0.6	3
45	Room-temperature synthesis, photoluminescence and photocatalytic properties of SnO nanosheet-based flowerlike architectures. Applied Physics A: Materials Science and Processing, 2012, 107, 437-443.	2.3	20
46	Monodisperse rutile TiO2 nanorod-based microspheres withÂvarious diameters: hydrothermal synthesis, formation mechanism and diameter- and crystallinity-dependent photocatalytic properties. Applied Physics A: Materials Science and Processing, 2011, 104, 149-158.	2.3	26
47	Synthesis and photocatalytic activity of porous polycrystalline NiO nanowires. Applied Physics A: Materials Science and Processing, 2011, 104, 69-75.	2.3	18
48	Synthesis, formation mechanism and electric property of hollow InP nanospheres. Applied Physics A: Materials Science and Processing, 2011, 104, 61-68.	2.3	5
49	Synthesis and size-dependent magnetic properties of single-crystalline hematite nanodiscs. Journal of Crystal Growth, 2011, 328, 62-69.	1.5	22
50	Hydrothermal synthesis and gas sensing properties ofÂsingle-crystalline ultralong ZnO nanowires. Applied Physics A: Materials Science and Processing, 2010, 98, 635-641.	2.3	43
51	The Ag+ induced solution–liquid–solid growth, photoluminescence and photocatalytic activity of twinned ZnSe nanowires. Applied Physics A: Materials Science and Processing, 2010, 98, 801-810.	2.3	8
52	Controllable synthesis and shape-dependent photocatalytic activity of ZnO nanorods with a cone and different aspect ratios and of short-and-fat ZnO microrods by varying the reaction temperature and time. Applied Physics A: Materials Science and Processing, 2010, 100, 1061-1067.	2.3	32
53	Vapor–liquid–solid growth and narrow-band ultraviolet photoluminescence of well-aligned GeO2 nanowire arrays withÂcontrollable aspect ratios. Applied Physics A: Materials Science and Processing, 2010, 100, 493-499.	2.3	12
54	Thermal oxide synthesis and characterization of Fe3O4 nanorods and Fe2O3 nanowires. Science in China Series B: Chemistry, 2009, 52, 599-604.	0.8	8

HEQING YANG

#	Article	IF	CITATIONS
55	Controlled growth and photoluminescence of highly oriented arrays of ZnO nanocones with different diameters. Science in China Series D: Earth Sciences, 2009, 52, 1264-1272.	0.9	6
56	In-situ growth and photoluminescence of β-Ga2O3 cone-like nanowires on the surface of Ga substrates. Science in China Series D: Earth Sciences, 2009, 52, 1712-1721.	0.9	6
57	Controlled synthesis and gas-sensing properties of hollow sea urchin-like α-Fe2O3 nanostructures and α-Fe2O3 nanocubes. Sensors and Actuators B: Chemical, 2009, 141, 381-389.	7.8	157
58	Synthesis of hollow microspheres constructed with $\hat{l}\pm$ -Fe2O3 nanorods and their photocatalytic and magnetic properties. Journal of Alloys and Compounds, 2009, 477, 90-99.	5.5	63
59	Controlled synthesis and magnetic properties of Fe3O4 walnut spherical particles and octahedral microcrystals. Science in China Series D: Earth Sciences, 2008, 51, 1911-1920.	0.9	16
60	Synthesis and photoluminescence of hollow microspheres constructed with ZnO nanorods by H2 bubble templates. Chemical Physics Letters, 2008, 455, 93-97.	2.6	26
61	Controlled Solvothermal Synthesis of Nanosheets, Nanobelts, and Ultralong Nanobelt Arrays with Honeycomb-Like Micropatterns of ZnSe on Zinc Substrate. Inorganic Chemistry, 2008, 47, 11950-11957.	4.0	31
62	Sol–Gel Synthesis and Photoluminescence of III-V Semiconductor InAs Nanocrystals Embedded in Silica Glasses. Journal of Nanoscience and Nanotechnology, 2005, 5, 786-789.	0.9	1
63	Sol–Gel Synthesis of Luminescent InP Nanocrystals Embedded in Silica Glasses. Journal of Nanoscience and Nanotechnology, 2005, 5, 1737-1740.	0.9	7